# 8.

# Corner radius effect in the thin-walled columns of regular polygon cross-section on the local buckling and load carrying capacity

It is a common observation that the thin-walled columns of flat walls are widely used in engineering practice. However, despite high strength materials applied for their manufacturing, those structures couldn't be fully exploit due to mostly low values of critical stress of a local buckling. In the stability of structures it is obvious that increasing the local stability could be gained by simple treatments: as thicker walls, stiffeners or by changing the cross-section shape. But those methods lead to making a structure larger and heavier. Nowadays, the optimization of the material distribution is the crucial factor during projecting and design process. It encourages to find the best coherence between a local buckling load or an ultimate load and cross section shape of specific structure without enlarging its cross-section area i.e. its total mass. As an example in [8.4] authors proof that the load carrying capacity of thin-walled multi-cell columns can be increased by changing their cross-section shape but not its entire area. Tillman and Williams [8.11] were searching for an agreement between the tests and the theory for the problems associated with defining the buckling loads of practical columns. The performed comparison tests gave results to be good in the main with theory. Camotim at all [8.2] applied the generalised beam theory (GBT) formulation to perform first-order and buckling analyses of arbitrary thin-walled members, namely members with cross-sections that combine closed cells with open branches. Królak at all [8.6] analysed multicell closed cross-section columns and girders to determine their critical load and postbuckling response. There isotropic structures were considered whereas in [8.4, 8.7] orthotropic properties of column walls were assumed. The same authors team investigated analogous problem in laboratory experiments to validate the previous analytical approach with satisfactory results [8.5]. The problem of an influence of corner radii of square cross-section short thin-walled columns on the buckling and postbuckling response was introduced in [8.9].

It should be emphasize that the question of the local buckling of thin-walled columns has a numerous and well-known literature and has been thoroughly investigated. In particular within the literature survey, one can find some studies presented the influence of a cross section shape i.e. open or closed, on the local

stability [8.3, 8.8]. However, one can still find issues worth to be studied. Authors of this work have been investigated a corner radius effect on the local buckling of thin-walled structures. For each considered regular cross-section shapes (i.e. triangular, square, regular pentagon or hexagon) different values of corner radii were applied taking into account a constant area of a column cross-section. This study appears to be some kind of an optimizing analysis of thin-walled members without fundamental formulation.

## 8.1. Introduction

During axial-compression of a plate thin-walled steel column of regular polygon cross-section (mainly column with an even number of walls - it is square, regular hexagon or octahedron), we can determine the local buckling critical stress from the formula valid for a long uniformly-compressed rectangular plate simply supported at all edges (Eq. 8.1) [8.3, 8.8, 8.13]

$$\sigma_{kr} = 4\frac{\pi^2 D}{\mathrm{b}_0^2 t} = \frac{\pi^2 E}{3\left(1-\nu^2\right)}\left(\frac{t}{b_0}\right)^2 \tag{8.1}$$

where: $E$ - Young's modulus of column material,
$\nu$ - Poisson's ratio,
$b_o$ - width of column single wall or a long rectangular plate,
$t$ - wall thickness (or plate thickness).

Assuming that for steel $E$ = 200 GPa, $\nu$ = 0.3 and $b_o$ = 1 m, $t$ = 1 mm, $t$ = 2 mm, $t$ = 3 mm and $t$ = 4 mm, respectively, we got the following results

$\sigma_{cr}$ = 0.723 MPa for $t$ = 1 mm,

$\sigma_{cr}$ = 2.894 MPa for $t$ = 2 mm,

$\sigma_{cr}$ = 6.507 MPa for $t$ = 3 mm,

$\sigma_{cr}$ = 11.57 MPa for $t$ = 4 mm.

As we can see, these are very small values of critical stresses in comparison to the structural steel yield limit. Thus, the strength mechanical properties of applied material cannot be fully utilized in considered columns [8.8].

## 8.2. The problem formulation

We consider the local stability and load carrying capacity of thin-walled columns of a regular polygon (equilateral triangle, square, regular pentagon, hexagon, heptagon, octahedron etc.) cross-section with corner radii. In the frame of this analysis critical stresses of local buckling and load carrying capacity of thin-walled columns of various (mentioned) cross-sections subjected to axial-compression are considered. Among these cross-sections there are some with introduced radius corner ($r \neq 0$) and some without radius corner (i.e. $r = 0$, $b = b_0$). For comparison reasons we assume that the material, column length, wall thickness and cross-section perimeter of all columns are the same. The radius of a corner between two adjacent walls could be changed between $0 \leq r_n \leq r_c$, where $r_c$ - radius of a circle with total circumference equal to a total perimeter of each considered of columns (it is the radius of cylindrical shell).

## 8.3. Column cross-section geometry description

In Fig. 8.1 some basic cross section dimensions of considered columns are presented and designated. They are respectively: $r_n$ - a corner radius of regular polygon columns, $b_{0n}$ - a single wall width of regular polygon cross section column with $n$ walls and with radius $r_n = 0$, $b_n$ - a flat wall element width ('net' width between radii) of regular polygon cross section with $n$ walls and a corner radius $r_n \neq 0$.

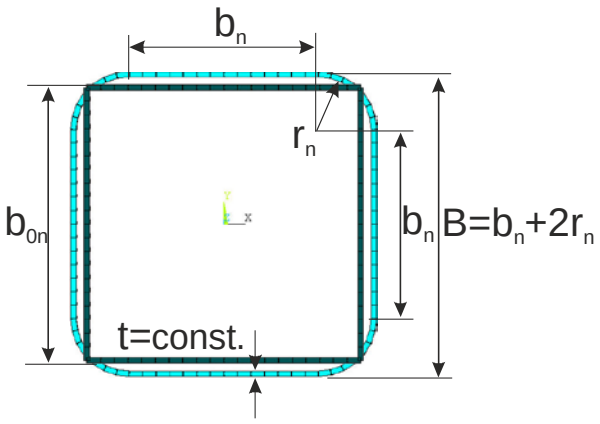


Fig. 8.1. Cross-section of a square section column with corner radii

We consider columns with a global number of walls $n = 3 \div 8$. The single wall width $b_{on}$ of any regular polygon without corner radii is referred to a square column cross-section ( $n = 4$ ), where a single wall width is marked as - $b_{04}$.

From the equality of a column perimeter it follows that $nb_{on} = 4b_{04}$. Therefore

$$b_{on} = 4b_{04}/n \tag{8.2}$$

After comparing perimeter of columns without corner radii and with corner radius $r_n$, we simply got $nb_{0n} = nb_n + 2\pi r_n$. From the later relationship it follows that

$$b_n = b_{0n} - \frac{2\pi}{n} r_n \tag{8.3}$$

For each of considered columns we obtain a cylindrical shell in the case when $b_n = 0$ - thus for walls without flat parts. This shell radius equals to

$$r_n = \frac{n}{2\pi} b_{0n} = \frac{2}{\pi} b_{04} \tag{8.4}$$

and it is identical for all considered columns (it is not dependable on *n* a total number of walls of regular polygon). Thus after a simple recalculation $r_n = 2/\pi\, b_{04} = 0.63662 b_{04}$ and therefore corner radius between adjacent walls could be changed between the limits of $0 \le r_n \le 0.63662 b_{04}$.

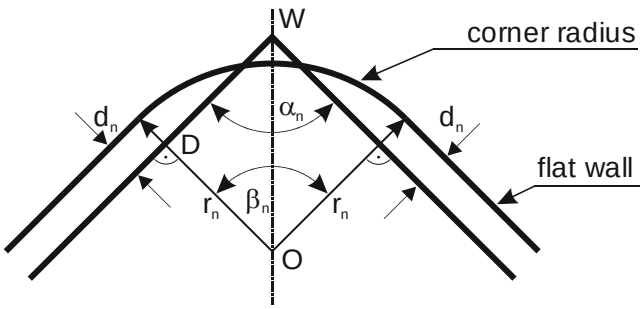


Fig. 8.2. Vertex geometry

In Fig. 8.2 an exemplary vertex of a regular polygon cross-section is shown. We indicate as $\alpha_n$ an angle between adjacent (corner) walls because this angle depends on *n* the number of column walls. For a regular polygon with *n* component walls we can define these distinctive angles as follows

$$\alpha_n = \pi - \frac{2\pi}{n} = \frac{\pi(n-2)}{n}$$

and also

$$\beta_n = \pi - \alpha_n = \frac{2\pi}{n}$$

In Fig. 8.2 the distance between flat part of a wall in the polygon with corner radius and without corner radius is denoted by $d_n$. As it is also shown in this figure, the length of segment $\overline{WD}$ equals to $\overline{WD} = \frac{1}{2}(b_{0n} - b_n) = \frac{\pi}{n} r_n$. Moreover, $r_n - d_n = \overline{WD} \cdot ctg\frac{\beta_n}{2}$, and finally one gets

$$d_n = r_n(1 - \frac{\pi}{n} ctg\frac{\pi}{n}) \tag{8.5}$$

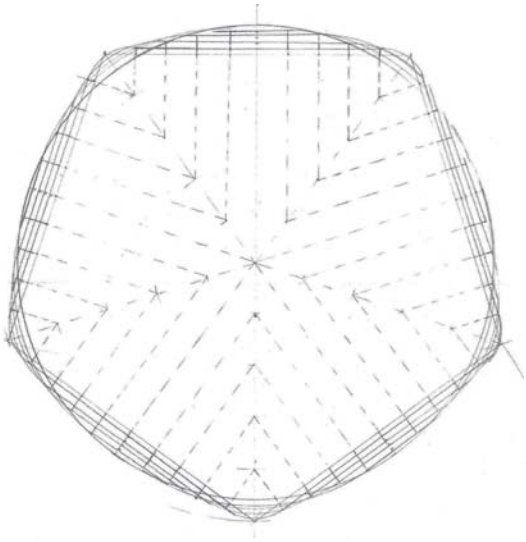

Fig. 8.3. Family of pentagon cross-sections

The position of the centre of any corner radius (point O in Fig. 8.2) counted from node W, results from a sine function of the angle $\frac{\beta_n}{2} = \frac{\pi}{n}$:

$$\sin\frac{\beta_n}{2} = \frac{\overline{WD}}{\overline{WO}} = \frac{\frac{\pi}{n} r_n}{\overline{WO}}$$

$$\overline{WO} = \frac{\frac{\pi}{n} \cdot r_n}{\sin\frac{\pi}{n}} = \frac{\pi \cdot r_n}{n \cdot \sin\frac{\pi}{n}}$$

To limit the range of considered possibilities the following data quantity has been assumed for computations:

- material modulus: $E = 2 \cdot 10^5$ MPa, $\nu = 0.3$;
- to maintain the same perimeter of all considered cross-section shapes it was assumed that the 'starting' width of a particular wall without corner radius is: $b_{03} = \frac{4}{3} m$, $b_{04} = 1m$, $b_{05} = \frac{4}{5} m = 0.8m$, $b_{06} = \frac{2}{3} m$, $b_{07} = \frac{4}{7} m$, $b_{08} = \frac{1}{2} m$, respectively.
- four wall thicknesses: $t_1 = 1\,mm$, $t_2 = 2\,mm$, $t_3 = 3\,mm$, $t_4 = 4\,mm$ - for all columns.

Among all possible corner radius values one can indicate few common radii lengths undependable on *n* number of column walls so the same dimension for particular column. Assuming again that $b_{04} = 1\,m$ these radii are given below and will be further applied for comparative juxtaposition:

$r_0 = 0$ - for columns without corner radius,

$r_1 = \frac{1}{5} r_c = \frac{1}{5} \cdot \frac{2}{\pi} b_{04} = \frac{2}{5\pi} b_{04} = \frac{2}{5\pi} 1 = 0.1273m$,

$r_2 = \frac{2}{5} r_c = \frac{4}{5\pi} b_{04} = \frac{4}{5\pi} 1 = 0.25465m$,

$r_3 = \frac{3}{5} r_c = \frac{6}{5\pi} b_{04} = \frac{6}{5\pi} 1 = 0.38197m$,

$r_4 = \frac{4}{5} r_c = \frac{8}{5\pi} b_{04} = \frac{8}{5\pi} 1 = 0.5093m$,

$r_5 = r_c = \frac{2}{\pi} b_{04} = \frac{2}{\pi} 1 = 0.63662m$ - a cylinder with radius $r_c$.

For the comparative analysis presented above radii values will be given in plots with numerical results.

## 8.4. Numerical model

To illustrate the impact of the corner radius insertion on the buckling stress and load carrying-capacity extent some computations were performed. The Finite Element Method was employed as an efficient tool for that purpose. The solution to the considered problem of a nonlinear buckling analysis of short thin-walled columns might be solved by application of a chosen variational method. However, the governing differential equations would be a mixture of a flat plate and a curved shell formulations with required junction conditions, what would lead to rather complex expressions. In a consequence the solution to that equation set would require numerical integration or generally numerical methods application. It all explains the FEM advantage and reasons of our choice to it application.

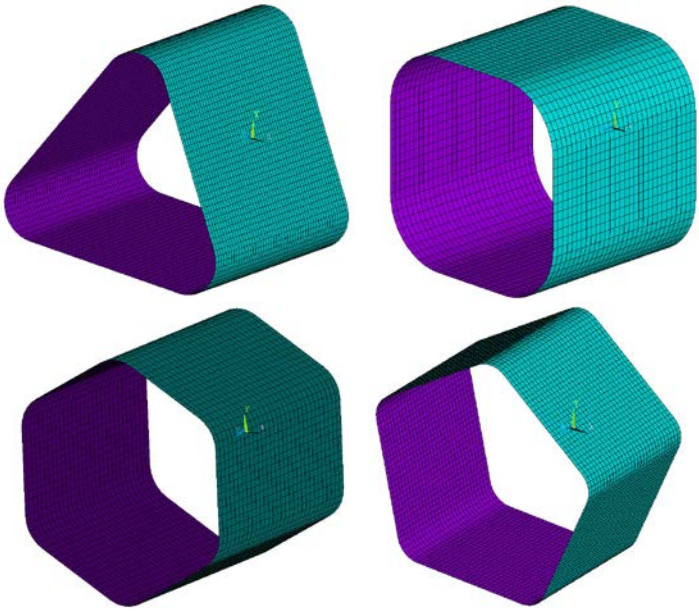

Fig. 8.4. Exemplary numerical models

The parametric numerical models of considered closed profile cross-section shapes were prepared in commercial package ANSYS [8.14] which is based on the FEM. The presented study concerns a thin-walled structure and the plane stress state, therefore a shell finite element was chosen to discretization and to formulate the finite element model. It was the SHELL181 - finite quadrilateral shell element of ANSYS software library. This element is suitable to nonlinear applications (strain and material) and is governed by the first order shear deformation theory in the case of multilayered composite cross-section. Each of

its four nodes has six degrees of freedom i.e. translations in the x, y, and z directions, and rotations about the x, y, and z-axes of a local coordinate system. Hereby the in-plane rotational (drill) stiffness is added at the nodes for solution stability. A penalty method is then used to relate this independent rotational degree of freedom about the normal to the shell surface with the in-plane components of displacement. That formulation offers excellent accuracy in curved-shell-structure simulations.

The developed numerical models of considered columns were discretized with an uniform mesh of finite elements (Fig. 8.4) and the full geometry was used to simulate assessed buckling and post-buckling response of a particular column. Despite of the existing geometrical symmetry of a considered structure, it was resigned from modelling only part of it to be able to analyse different deformation modes which could be lost in opposite case. The total number of finite elements approached ten thousands. It was a series of additional tests performed to check if the produced finite element model gives a reliable representation of the structure being analyzed. These tests are not described here due to limited scope of the paper.

The boundary conditions at loaded column edges followed the analytical assumption of simply supported type (Fig. 8.5). They were attained through constrained displacement of model edges in normal to a wall surface direction. For the limit shape i.e. cylindrical columns not only the radial but tangential displacements of column loaded edges were restricted. To fulfil additionally the condition of loaded edges being rectilinear the coupling constrains were introduced. Therefore, the applied system of displacement constrains allowed a replication of a column edge behaviour of a classical structural strength approach. It recalls also the standard conditions during a static compression test in a strength test machine.

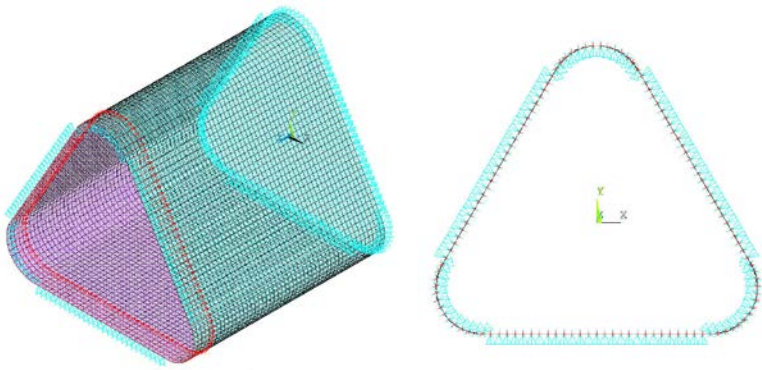

Fig. 8.5. Simply support BC defined in FEM model

Conducted analysis concerned an axial compression of studied short closed cross-section profiles/columns thus the loading was obtained by uniform nodal force distribution along 'upper' column edge where the 'lower' one was constrained against axial displacement.

The main interest of a nonlinear buckling analysis was the load carrying-capacity of an individual column which was preceded by the linear eigenbuckling analysis. From the first one, the critical load was determined as well as the first buckling mode. Obtained in this way eigenbuckling mode was introduced into the numerical model as initial imperfection. The eigenmode mapping technique was here applied. The magnitude of this out of flatness imperfection referred to a column wall thickness was in the range of 0.01÷0.1. The full Newton-Raphson iteration procedure was used as the incremental technique in the finite element structural analysis [8.1].

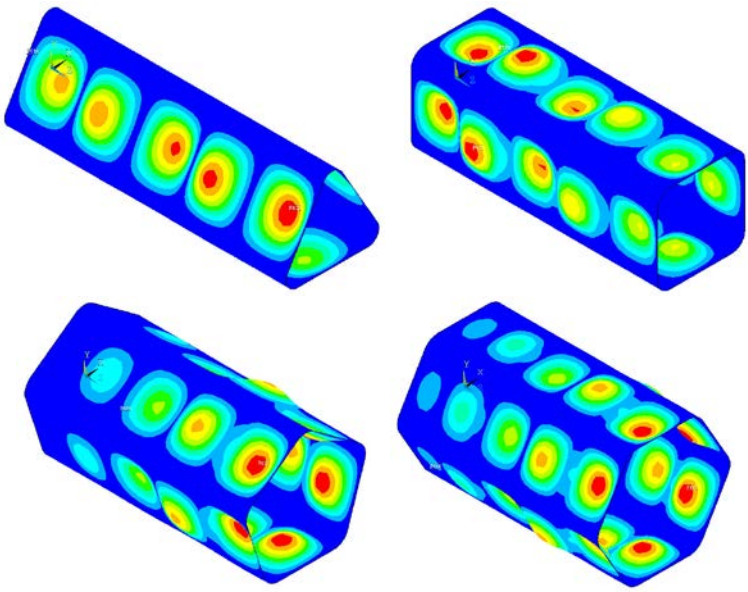

Fig. 8.6. First buckling modes for $b_{04}$ = 500 mm and equal $r$ length

The material model assumed in computations was defined by a bilinear characteristic with isotropic hardening. The static yield limit was taken as equal to $\sigma_y$ = 200 MPa with a tangent modulus $E_t$ = 2000 MPa, with the Young's modulus and Poisson ratio defined within the text above. Some considerations of applying the Needelman-Tvergard formula for approximation of material characteristic [8.10] or an input of a real material characteristic as multi-linear curve to eliminate the abrupt slope change in bilinear material description were

performed but their results did not improve the numerical process in a visible way and were skipped therefore. The yield surface was established with Huber-Mises-Hencky criterion hence the same yield stresses value in uniaxial tension and compression for ductile isotropic material was assumed.

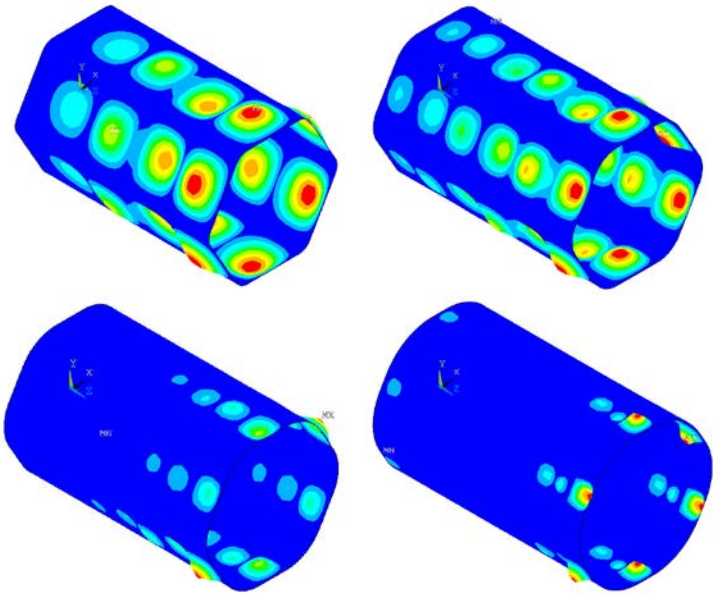

Fig. 8.7. First buckling modes of hexagon cross-section column for a series of $r$ length (0.2; 0.4;…0.8 of $r_c$)

## 8.5. Results of buckling stress computations

A lot of numerical analysis was performed with reference to four chosen cross-section shapes of thin-walled columns. These were regular polygons, i.e. equilateral triangle, square, regular polygon and regular hexagon. For comparison reasons it was assumed the equal perimeter of each polygon and then the formulas for the length of particular polygon side - defined above within the data for computations - were fulfilled. Two perimeter lengths were considered 4m and 2m, with four cases of column wall thickness. For particular column cross-section type a series of computations were performed where the buckling load - buckling stress, buckling modes and the load carrying-capacity were determined. To focus the attention on a local buckling phenomenon the total length of all considered columns were assumed three times a side length of a considered regular polygon. Thus all investigated thin-walled profiles were

of a short column class. Exemplary results are presented below in the following graphs and figures.

Within the first step of buckling analysis it was critical load determined as well as buckling modes. Some exemplary first modes of considered column shapes are presented in Figs. 8.6 and 8.7. In Fig. 8.6 there are presented buckled shapes of all profile cross-section types when the reference $b_{04} = 0.5\,m$ and the same value of corner radius $r_n = b_{04}/2\pi$ was assumed. One can observe the same number of halve waves along all column walls with visible modulation effect of buckles magnitude between loaded column ends. This effect is more pronounced when a cross-section shape tends to a cylinder (see Fig. 8.7). The length of a single buckle is shorter than $b_{0n}$ the flat part of a column wall. The very characteristic of detected modes is the fact that despite the cross-section shape and corner radius dimension, buckles occurred only throughout the flat part of walls. Buckling deformations of curved parts of column walls were never observed.

The predictable effect of buckling wave number and length connected with the increase of corner radius length is presented in Fig. 8.7. It corresponds to the previous conclusion that the width of a flat part of column wall influences the length thus a number of buckles along the column length. Also the modulation effect is visible too. However, for almost cylindrical columns the few first eigenbuckling values are very close each other (difference up to 5%) and their modes are similar with small difference in buckles magnitude only.

The impact of corner radius on the buckling load is presented on plots in subsequent figures for different juxtapositions.

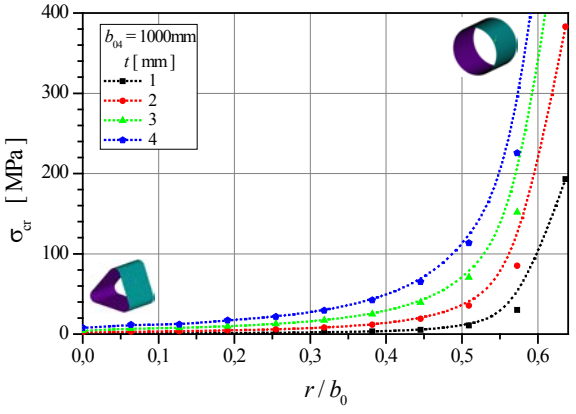


a)

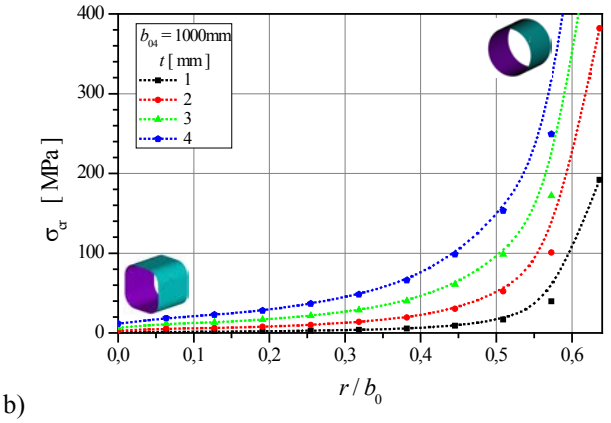


b)

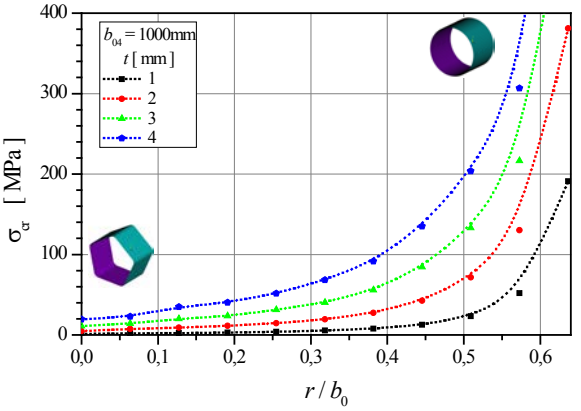


c)

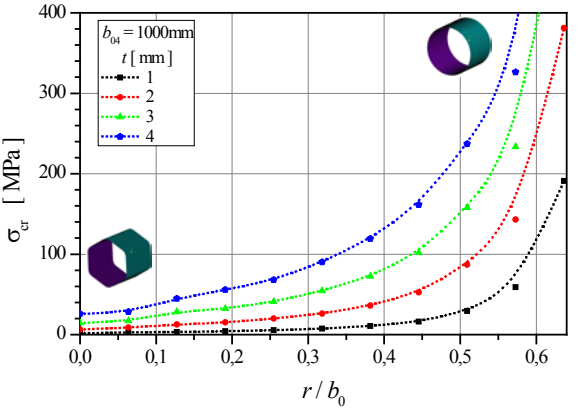


d)

Fig. 8.8. Critical stress value as a function of corner radius value for different cross-section shapes of $3\times b_{0n}$ columns

In Fig. 8.8 there are charts presenting the influence of corner radius length on the critical stress value increase for columns of four chosen cross-section shapes where the reference width of square cross-section wall is equal to $b_{04}=1\,m$. The pronounced jump of critical stress value between regular polygon and cylindrical cross-section is up to almost 400 times for regular triangle of $t_1=1\,mm$. This effect decreases when the number of polygon walls increases as well as the wall thickness does. The increasing effect of stress value is observed even for low dimensions of corner radii for polygons of greater number of walls whereas for triangle or square is visible for cross-section shapes closer to cylindrical shell.

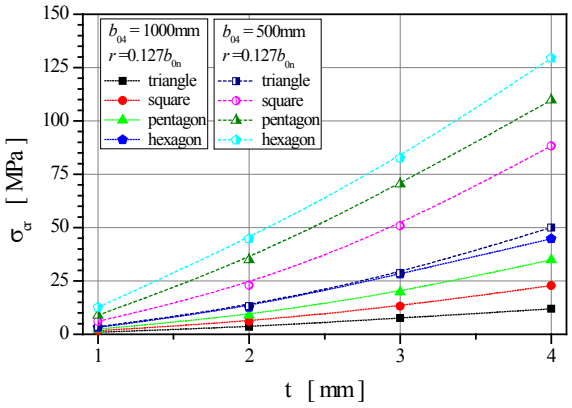


a)

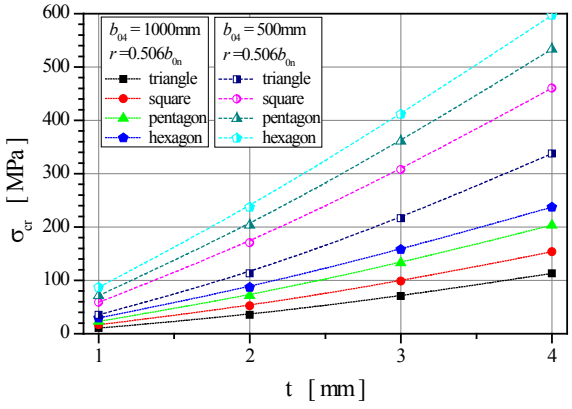


b)

Fig. 8.9. Critical stress value as a function of wall thickness for different corner radius values and cross-section shapes

Similar conclusions are valid for columns which reference cross-section perimeters differ (are greater or lower) to $4 \times b_{04} = 4\ m$. Then the critical stress relationship for regular polygon column and cylindrical column are in similar relationships as the their perimeters are to $4 \times b_{04} = 4\ m$.

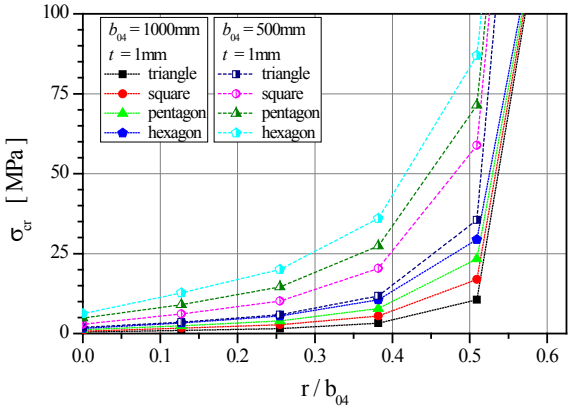


a)

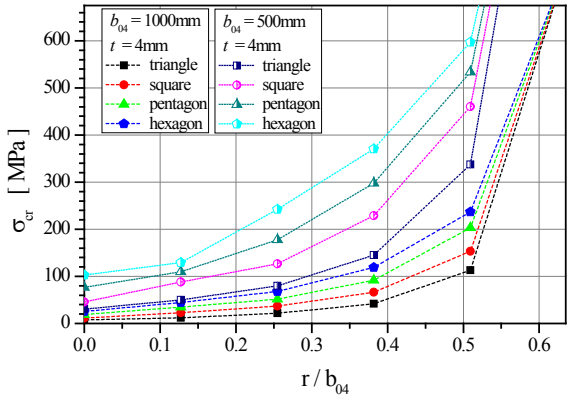


b)

Fig. 8.10. Critical stress value as a function of corner radius values for different cross-section shapes

Analyzing an impact of corner radius introduction between adjacent column walls on the buckling load one can compare this effect when changing the cross-section shape for constant wall thickness and the same perimeter length. From Fig. 8.9 it is visible that this effect is connected in greater degree with number of column walls (see triangle and hexagon) and it is more efficient for bigger corner radius length. However, the increase of critical stress value for the column of triangle cross-section when compared to a hexagon cross-section is greater for

thinner walls (i.e. $t_1 = 1\,mm$) than thicker on approximately 30%. This statement can also be referred to a shorter perimeter case and is more potent for a shorter radii (Fig. 8.9a). The changes in inclinations of the lines on the graphs in Fig. 8.9 are grater for an increasing number of column walls.

The conclusions drawn above are again confirmed by both scatter plots in Fig. 8.10, where exemplary results for two limit wall thicknesses $t_1 = 1\,mm$ and $t_1 = 4\,mm$ are presented. Despite the widespread ranges of critical stress absolute values for increasing corner radius dimension the relative relations between the buckling loads vary in a narrower range. However these ranges are broader for shorter perimeter length multiwall cases.

Table 8.1. Critical load and ultimate load for some column cases

| pentagon | $t$ = 1 mm | | $t$ = 2 mm | | $t$ = 3 mm | | $t$ = 4 mm | |
|---|---|---|---|---|---|---|---|---|
| $r/b_{04}$ | $\sigma_{cr}$ [MPa] | $\frac{N_{ult}}{N_{cr}}$ | $\sigma_{cr}$ [MPa] | $\frac{N_{ult}}{N_{cr}}$ | $\sigma_{cr}$ [MPa] | $\frac{N_{ult}}{N_{cr}}$ | $\sigma_{cr}$ [MPa] | $\frac{N_{ult}}{N_{cr}}$ |
| 0 | 4.8 | 5.691 | 19.2 | 2.690 | 43.1 | 1.760 | 76.4 | 1.329 |
| 0.063662 | 7.3 | 4.121 | 22.8 | 2.304 | 46.5 | 1.640 | 79.1 | 1.277 |
| 0.127324 | 9.0 | 4.028 | 34.9 | 1.869 | 70.4 | 1.633 | 109.8 | 1.054 |
| 0.190986 | 11.2 | 3.489 | 40.2 | 1.737 | 86.8 | 1.224 | 151.3 | 1.012 |
| 0.254648 | 14.5 | 2.843 | 51.5 | 1.500 | 105.3 | 1.167 | 177.5 | 0.999 |
| 0.31831 | 19.4 | 2.311 | 68.2 | 1.291 | 139.6 | 1.033 | 226.2 | 0.834 |
| 0.381972 | 27.3 | 1.830 | 91.6 | 1.098 | 184.0 | 0.896 | 297.6 | 0.635 |
| 0.445634 | 42.6 | 1.597 | 135.0 | 1.033 | 256.9 | 0.726 | 401.6 | 0.485 |
| 0.509296 | 71.4 | 1.346 | 203.4 | 0.867 | 360.8 | 0.532 | 533.5 | 0.366 |
| 0.572958 | 130.2 | 1.075 | 306.5 | 0.617 | 491.7 | 0.394 | 681.0 | 0.286 |

For assumed column overall dimensions and shapes in the most cases the calculated critical stress values are very low when compared to the yield limit for assumed structural steel. Thus the load carrying-capacity of these columns gives a broad reserve of loading. Higher critical stress values were determined for thicker column walls and greater corner radius dimensions what makes a column stiffer. The later values determined in the linear eigenbuckling analysis are in many cases above the yield limit for assumed material properties. In the nonlinear buckling analysis - in a geometrical approach and in terms of a real material characteristic, a critical load is restricted by the structural steel yield strength. This type of analysis requires too two steps and time consuming computations. Hence the assessment of an impact of corner radii effect on the ultimate load of considered columns was performed for limited number of

structures. The exemplary results of this analysis are summarized in Table 8.1. Nevertheless, the drawn conclusions can be extended to all investigated short columns of regular polygon cross-sections.

The representative results presented in Table 8.1 were obtained for a column of a pentagonal cross-section with the reference width of a single wall $b_{04} = 0.5\,m$, what makes $b_{05} = 0.4\,m$ and the profile total length equal to $3 \times b_{04} = 1.2\,m$. A critical stress determined for a thin wall solution of analysed columns allows a post-buckling work of a column in a much wider range than for thicker walls structure. The available excess of loading up to the ultimate load reaches few times the critical stress. This relationship reduces with the increase of corner radius length and with the wall thickness. Then from obvious reasons the quotient $N_{ult}/N_{cr}$ of ultimate force and critical force is lower than one. Here again it should be emphasized that also in the post-buckling range local buckling deformations are observed over the 'flat' parts of column walls. For a small reserve of axial compression ($N_{ult}/N_{cr}$ a bit greater than 1) local buckles follow the eigenbuckling pattern and enter the curved parts of column walls in deep post-buckling range. This phenomenon is shown in Fig. 8.11. In the far post-buckling stage the wall deformations are shifted towards the loaded edge and form deep inside deflections. Due to relatively flat hardening part of stress-strain diagram assumed for computations ($E_t$ = 2000 MPa) the equivalent stress value gained 221 MPa in the region close to the column loaded end.

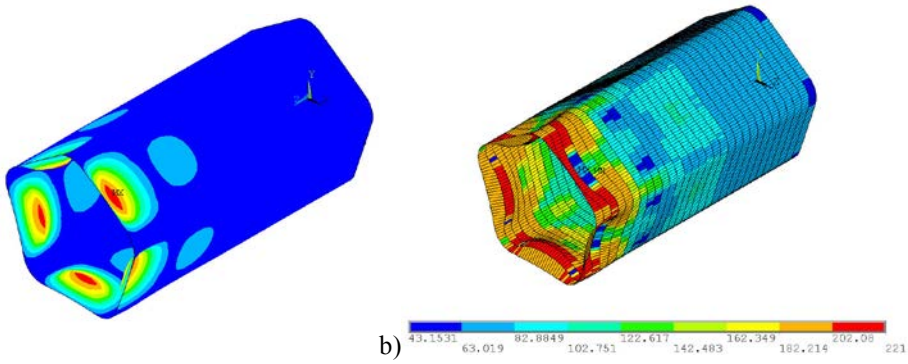


Fig. 8.11. a) Post-buckling displacements,
b) stress map of a short pentagon column

## 8.6. Conclusions

The performed investigations confirmed the impact of corner radii solution on the thin-walled column local buckling load value. The buckling strength of

a column can be controlled (increased) by introduction of a curved radial junction of adjacent walls. This statement is valid for different cross-section shapes. However, the increase effect is more visible for columns of greater number of walls. In the performed FEM computations, where the buckling shapes of analysed structures were possible to watch both at critical load state as well as in the post-buckling range, it has been never observed buckles over curved parts of column walls, only flat strips of walls exhibited deformations.

Application of medium values of corner radii for columns of thinner walls has given better effect for ultimate load surplus. For thicker walls the yield stress value was crucial for restricting the axial column load. This effect was enhanced by greater dimension of corner radius.

Columns of greater number of walls exhibit better properties as it goes on local buckling load and react in a more profitable or useful way on the corner radius introduction.

## 8.7. References


8.1 Bathe K.J., Finite element procedure, Prentice-Hall Inc., New Jersey 1996.

8.2 Goncalvesa R., Dinis P.B., Camotim D., GBT formulation to analyse the first-order and buckling behaviour of thin-walled members with arbitrary cross-sections, Thin-Walled Structures, Vol. 47, 5, 2009, pp. 583-600.

8.3 Królak M. (Ed.), Buckling, postbuckling and load carrying capacity of thin-walled orthotropic structures, Monographs, Technical Univ. of Lodz 1995 (*in Polish*).

8.4 Królak M., Kowal-Michalska K., Stability and ultimate load of multi-cell orthotropic columns subjected to compression, in Shell Structures Theory and Application, Pietraszkiewicz W., Szymczak Cz. (eds.), Taylor&Francis Gr., London 2006, pp. 235-239.

8.5 Królak M., Kowal-Michalska K., Mania R.J, Świniarski J., Experimental tests of stability and load carrying capacity of compressed thin-walled multi-cell columns of triangular cross-section Thin-Walled Struct.,Vol. 45, 10-11, 2007, pp. 883-887.

8.6 Królak M., Kowal-Michalska K., Mania R.J, Świniarski J., Stability and load carrying capacity of multicell thin-walled columns of rectangular cross-section, J. of Theoretical and App. Mechanics, 47, 2, 2009, pp. 435-456.

8.7 Królak M., Mania R.J., Critical and postcritical behavior of thin-walled multicell column of open profile, Mechanics and Mechanical Eng., Vol. 14, No. 2, 2010, pp. 281-290.

8.8 Królak M., Mania R. J. (eds), Stability of thin-walled plate structures, Vol. 1 of Statics, Dynamics and Stability of Structures, Series of Monographs, Technical Univ. of Lodz 2011.

8.9 Królak M., Mania R.J., Kamocka M., Corner radius effect in thin-walled square section columns on the local buckling of walls under axial compression, Proceedings of the XIV Symp. on the Stability of Struct., Mania R.J. (ed.), 2015, pp. 63-64.

8.10 Mania R.J., Kowal-Michalska K., Parametryczna analiza stateczności dynamicznej konstrukcji cienkościennych Metodą Elementów Skończonych, in: Analizy numeryczne wybranych zagadnień mechaniki, Niezgoda T. (ed.), Wyd. WAT, Warszawa 2007, pp. 227-243 (in Polish).

8.11 Tillman S.C., Williams A.F., Buckling under compression of simple and multicell plate columns, Thin-Walled Structures, Vol. 8, 2, 1989, pp. 147-161.

8.12 Timoshenko S., Gere J., Theory of elastic stability, McGraw-Hill, 1961.

8.13 Volmir A.S., Ustoiczivost deformirujemych system, Nauka, Moskwa 1967.

8.14 ANSYS Help, Release 15.0, SAS IP, Inc., 2013.